

Exploring the QGP phase above the deconfinement temperature in pp and $A - A$ collisions at LHC energies

Aditya Nath Mishra,^a Guy Paic,^b Carlos Pajares,^c Rolf P Scharenberg,^d and Brijesh K Srivastava^{d,1}

^aWigner Research Center for Physics, H-1121 Budapest, Hungary

^bInstituto de Ciencias Nucleares, Universidad Nacional Autónoma de México, Apartado Postal 70-543, México Distrito Federal 04510, México

^cDepartamento de Física de Partículas, Universidade de Santiago de Compostela and Instituto Galego de Física de Altas Enerxías(IGFAE), 15782 Santiago, de Compostela, Spain

^dDepartment of Physics and Astronomy, Purdue University, West Lafayette, IN-47907, USA

E-mail: Aditya.Nath.Mishra@cern.ch, Guy.Paic@cern.ch,
carlos.pajares@usc.es, schrnrbg@purdue.edu, brijesh@purdue.edu

ABSTRACT: In the present work we have analyzed the transverse momentum spectra of charged particles in high multiplicity pp collisions at LHC energies $\sqrt{s} = 5.02$ and 13 TeV published by the ALICE Collaboration using the Color String Percolation Model (CSPM). For heavy ions Pb-Pb at $\sqrt{s_{NN}} = 2.76$ and 5.02 TeV along with Xe-Xe at $\sqrt{s_{NN}} = 5.44$ TeV have been analyzed. The initial temperature is extracted both in low and high multiplicity events in pp collisions. For $A - A$ collisions the temperature is obtained as a function of centrality. A universal scaling in the temperature from pp and $A - A$ collisions is obtained when multiplicity is scaled by the transverse interaction area. For the higher multiplicity events in pp collisions at $\sqrt{s} = 5.02$ and 13 TeV the initial temperature is above the universal hadronization temperature and is consistent with the creation of deconfined matter. From the measured energy density ϵ and the temperature the dimensionless quantity ϵ/T^4 is obtained. Our results agree with the Lattice Quantum Chromo Dynamics simulations (LQCD) up to ~ 210 MeV and beyond that there is a sharp increase in ϵ/T^4 , reaching the ideal gas of quarks and gluons value of $\epsilon/T^4 = 16$ at temperature ~ 230 MeV. It has been argued that there exists a three-phase structure of matter in QCD : hadronic matter, a plasma of deconfined massive quarks and a plasma of massless quarks and gluons with full color deconfinement and chiral symmetry restoration [1]. Our results suggests that chiral symmetry restoration occurs at a temperature ~ 210 MeV.

¹Corresponding author.

Contents

1	Introduction	1
2	Clustering of color sources	2
3	Determination of color suppression factor $F(\xi)$	4
4	Connection between $F(\xi)$ and temperature	7
5	Thermalization	11
6	Energy density	13
7	Two temperatures	16
8	Degrees of freedom DOF	16
9	Discussion	17
10	Conclusions	17
11	Acknowledgments	18

1 Introduction

The Quantum Chromodynamics (QCD) phase diagram is closely related to the history of the universe and can be probed by heavy ion collisions. Of particular interest in the heavy ion collision experiments are the details of the deconfinement and chiral transitions which determine the QCD phase diagram. One of the main challenges of the field is to simultaneously determine the initial temperature and the energy density of the matter produced in a collision and hence the number of thermodynamic degrees of freedom (DOF) [2].

Several interesting features related to the *QGP* formation e.g., long range rapidity correlations, the so called “ridge”, elliptic flow and strangeness enhancement seen in heavy ion collisions are also observed in high multiplicity *pp* collisions at LHC energies [3–7].

The objective of the present work is to obtain the thermodynamic properties like initial temperature and the degrees of freedom (DOF) in *pp*, Pb-Pb, and Xe-Xe collisions at LHC energies by analyzing the published ALICE data on the transverse momentum spectra of charged hadrons [8–11] using the framework of clustering of color sources (CSPM) [12]. A letter was published using the limited sets of data [13].

This approach has been successfully used to describe the initial stages in the soft region in high energy nucleus-nucleus and nucleon-nucleon collisions [14–24]. The CSPM is in fact different from the hydrodynamics picture and is more in line with other studies where the interaction among strings[25–27] or the domain color structure [28, 29] is taken into account. Lattice Quantum Chromo Dynamics simulations (LQCD) indicate that the non-perturbative region of hot QCD matter extends up to temperature of 400 MeV, well above the universal hadronization temperature [30].

The paper is organized as follows: section 2 describes the phenomenology of the color string percolation model. The measurement of color suppression factor $F(\xi)$ and its relation to temperature are presented in sections 3 and 4. Sections 5 to 8 describe thermalization, energy density, and degrees of freedom.

2 Clustering of color sources

Multiparticle production is currently described in terms of color strings stretched between the projectile and the target, which decay into new strings through color neutral $q - \bar{q}$ pairs production and subsequently hadronize to produce the observed hadrons [12, 31, 32]. Color strings may be viewed as small areas in the transverse plane filled with color field created by colliding partons. In terms of gluon color field they can be considered as the color flux tubes stretched between the colliding partons. The mechanism of particle creation is the Schwinger QED_2 mechanism and is due to the color string breaking. String breaking proceeds in an iterative way until they come to objects with masses comparable to hadron masses, which can be identified with observable hadrons by combining the produced flavor with statistical weights [33, 34]. The Schwinger mechanism has also been used in the decay of color flux tubes produced by the quark-gluon plasma for modeling the initial stages in heavy ion collisions [35, 36].

With growing energy and size of the colliding system, the number of strings grows, and they start to overlap, forming clusters, in the transverse plane very much similar to disks in two dimensional percolation theory as shown in Fig. 1 [37, 38]. At a certain critical density, a macroscopic cluster appears that marks the percolation phase transition. The interaction between strings occurs when they overlap and the general result, due to the SU(3) random summation of charges, is a reduction in multiplicity and an increase in the string tension, hence increase in the average transverse momentum squared, $\langle p_T^2 \rangle$. This is the Color String percolation Model (CSPM) [31, 32]. We assume that a cluster of n strings that occupies an area of S_n behaves as a single color source with a higher color field \vec{Q}_n corresponding to the vectorial sum of the color charges of each individual string \vec{Q}_1 . The resulting color field covers the area of the cluster. As $\vec{Q}_n = \sum_1^n \vec{Q}_1$, and the individual string colors may be oriented in an arbitrary manner with respect to each other, the average $\vec{Q}_{1i}\vec{Q}_{1j}$ is zero, and $\vec{Q}_n^2 = n\vec{Q}_1^2$. This results in the suppression of the multiplicity and the enhancement of $\langle p_T^2 \rangle$. Knowing the color charge \vec{Q}_n one can obtain the multiplicity μ_n and the mean transverse momentum squared $\langle p_T^2 \rangle_n$ of the particles produced by a cluster of n strings [32]

$$\mu_n = \sqrt{\frac{nS_n}{S_1}}\mu_1; \quad \langle p_T^2 \rangle_n = \sqrt{\frac{nS_1}{S_n}}\langle p_T^2 \rangle_1 \quad (2.1)$$

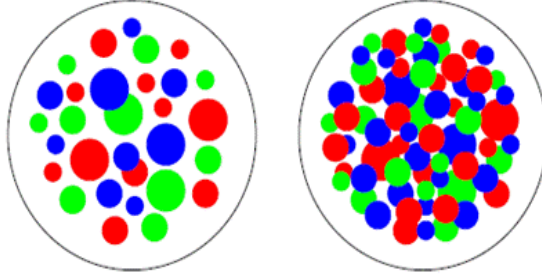


Figure 1. Partonic cluster structure in the transverse collision plane at low (left) and high (right) parton density [38].

Table 1. Event multiplicity classes based on the number of tracklets ($N_{SPDtracklets}$) within $|\eta| < 0.8$ for pp collisions. For V0M it covers the region $2.8 < \eta < 5.1$ and $-3.7 < \eta < -1.7$. In both cases $\langle dN_{ch}/d\eta \rangle$ is given in the region $|\eta| < 0.8$ [8–11].

System	pp 13 TeV	pp 13 TeV	pp 5.02 TeV	pp 5.02 TeV	pp 7 TeV
	$N_{SPDtracklets}$	V0M	$N_{SPDtracklets}$	V0M	V0M
Multiplicity class	$\langle dN_{ch}/d\eta \rangle$				
I	54.1	26.6	-	19.2	21.3
II	44.6	20.5	34.6	15.1	16.5
III	38.9	16.7	29.9	12.4	13.5
IV	34.1	14.3	26.2	10.7	11.5
V	29.3	12.6	22.4	9.47	10.1
VI	24.5	10.6	18.5	8.04	8.45
VII	19.5	8.46	14.6	6.56	6.72
VIII	14.4	6.82	10.6	5.39	5.40
IX	9.03	4.94	6.58	4.05	3.90

where μ_1 and $\langle p_T^2 \rangle_1$ are the mean multiplicity and $\langle p_T^2 \rangle$ of particles produced from a single string with a transverse area $S_1 = \pi r_0^2$, where r_0 is the string radius. For strings just touching each other $S_n = nS_1$, and $\mu_n = n\mu_1$, $\langle p_T^2 \rangle_n = \langle p_T^2 \rangle_1$. When strings fully overlap, $S_n = S_1$ and therefore $\mu_n = \sqrt{n}\mu_1$ and $\langle p_T^2 \rangle_n = \sqrt{n}\langle p_T^2 \rangle_1$, so that the multiplicity is maximally suppressed and the $\langle p_T^2 \rangle_n$ is maximally enhanced. This implies a simple relation between the multiplicity and transverse momentum $\mu_n \langle p_T^2 \rangle_n = n\mu_1 \langle p_T^2 \rangle_1$, which means conservation of the total transverse momentum produced.

In the thermodynamic limit, one obtains an analytic expression [31, 32]

$$\left\langle \frac{nS_1}{S_n} \right\rangle = \frac{\xi}{1 - e^{-\xi}} \equiv \frac{1}{F(\xi)^2} \quad (2.2)$$

where $F(\xi)$ is the color suppression factor and $\xi = \frac{N_s S_1}{S_N}$ is the percolation density parameter.

Equation 2.1 can be written as $\mu_n = nF(\xi)\mu_1$ and $\langle p_T^2 \rangle_n = \langle p_T^2 \rangle_1 / F(\xi)$. The critical cluster which spans S_N , appears for $\xi_c \geq 1.2$ [37, 38].

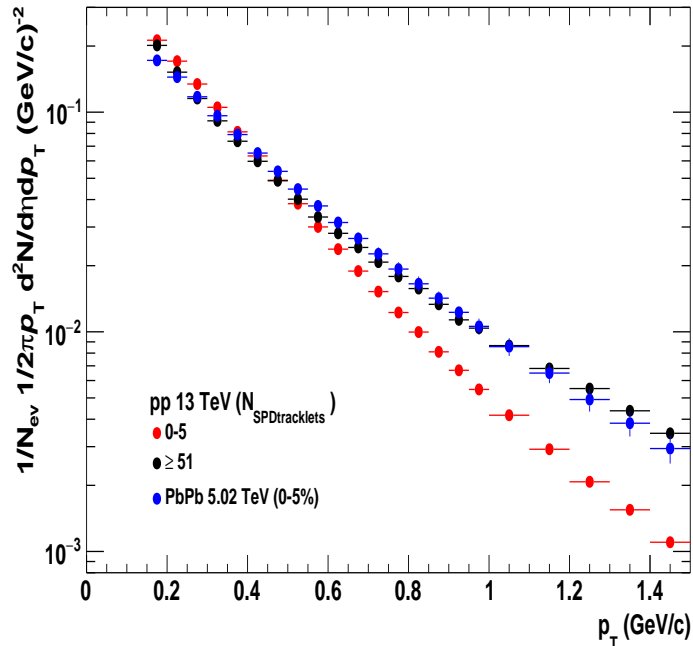


Figure 2. Transverse momentum spectra of charged particles from ALICE experiment in pp collisions at $\sqrt{s} = 13$ TeV for two different multiplicity cuts $N_{SPDtracklets} \geq 51$ (purple solid circle) and $N_{SPDtracklets} < 5$ (red solid circle) [8]. Pb-Pb collision spectra at $\sqrt{s_{NN}} = 5.02$ TeV for 0-5% centrality is shown as blue solid circle [10].

It is worth noting that CSPM is a saturation model similar to the Color Glass Condensate (CGC), where $\langle p_T^2 \rangle_1 / F(\xi)$ plays the same role as the saturation momentum scale Q_s^2 in the CGC model [39, 40]. Saturation results from the overcrowding in impact parameter of low x partons of a boosted hadrons or nucleus, leading to the appearance of a scale, Q_s^2 . This is the basic idea of CGC. For example, the particle density in CSPM is given by

$$\frac{dn}{dy} \sim (1 - e^{-\xi})^{1/2} N_{part}. \quad (2.3)$$

In CGC particle density is related to the coupling constant $\alpha_s(Q_s^2)$,

$$\frac{dn}{dy} \sim \frac{1}{\alpha_s(Q_s^2)} N_{part}. \quad (2.4)$$

In both cases particle density increases with the number of participants N_{part} [40]. The correction to the N_{part} scaling in the CGC is due to the occupation number given by $1/\alpha_s$ which give rise to a $\log(N_{part})$ dependence. In the CSPM, the correction is given by the factor $(1 - \exp(-\xi))^{1/2}$ (Eq.(2.3)), which is also a measure of the occupation, indeed is the fraction of the collision area occupied by strings.

3 Determination of color suppression factor $F(\xi)$

In the present work we have extracted the color suppression factor $F(\xi)$ in high multiplicity events in pp collisions using ALICE data from the transverse momentum spectra of charged

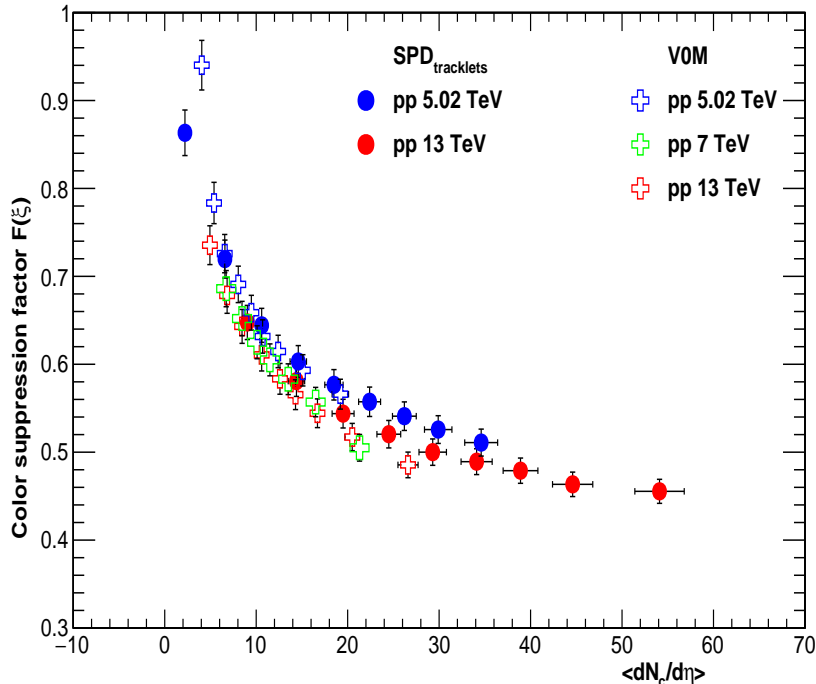


Figure 3. Color Suppression Factor $F(\xi)$ in pp collisions vs $\langle dN_{ch}/d\eta \rangle$ for $SPD_{tracklets}$ and V0M event multiplicity classes. For pp collisions at $\sqrt{s} = 7$ TeV only V0M event multiplicity classes are available. $\langle dN_{ch}/d\eta \rangle$ is the charged particle multiplicity covering the kinematic range $|\eta| < 0.8$ and transverse momentum $p_T = 0.15 - 20$ GeV/c [8].

particles at $\sqrt{s} = 5.02$ and 13 TeV [8]. ALICE has obtained the transverse momentum distribution for two multiplicity estimators which cover different pseudorapidity regions. The estimators are based on either the total charged deposited in the forward detector (covering the pseudorapidity regions $2.8 < \eta < 5.1$ and $-3.7 < \eta < -1.7$) V0M or on the number of tracks in the pseudorapidity region $|\eta| < 0.8$ $N_{SPDtracklets}$. Table 1 shows the event multiplicity classes based on V0M and $N_{SPDtracklets}$ for pp collisions at $\sqrt{s} = 5.02$ and 13 TeV [8]. Table 1 also shows the various multiplicity classes based on V0M estimator for pp at $\sqrt{s} = 7$ TeV [9].

Figure 2 shows a transverse momentum spectra for two multiplicity cuts at $\sqrt{s} = 13$ TeV in pp collisions and Pb-Pb at $\sqrt{s_{NN}} = 5.02$ TeV for 0-5 % centrality. The spectra becomes harder for higher multiplicity cuts. This is due to the fact that high string density color sources are created in the higher multiplicity events. To evaluate the initial value of $F(\xi)$ from data in high multiplicity events in pp collisions, a parameterization of the experimental data of p_T distribution in low energy pp collisions at $\sqrt{s} = 200$ GeV was used [14]. The charged particle spectrum is described by a power law [12]

$$d^2N_c/dp_T^2 = a/(p_0 + p_T)^\alpha, \quad (3.1)$$

where a is the normalization factor, p_0 and α are fitting parameters with $p_0 = 1.98$ and α

= 12.87 [14]. This parameterization is used in high multiplicity pp collisions to take into account the interactions of the strings [12]. The color suppression factor $F(\xi)$ encodes the effects of the interaction among strings once they overlap. The parameter p_0 in Eq. (3.1) is for independent strings and gets modified

$$p_0 \rightarrow p_0 \left(\frac{\langle nS_1/S_n \rangle_{pp}^{mult}}{\langle nS_1/S_n \rangle_{pp}} \right)^{1/4}, \quad (3.2)$$

$$\frac{d^2 N_c}{dp_T^2} = \frac{a}{(p_0 \sqrt{F(\xi)_{pp}/F(\xi)_{pp}^{mult}} + p_T)^\alpha}, \quad (3.3)$$

where $F(\xi)_{pp}^{mult}$ is the multiplicity dependent color suppression factor. In pp collisions $F(\xi)_{pp} \sim 1$ at low energies due to the low overlap probability. The spectra were fitted using Eq. (3.3) in the softer sector with p_T in the range 0.12-1.0 GeV/c. In the thermodynamic limit the color suppression factor $F(\xi)$ is related to the percolation density parameter ξ [12]

$$F(\xi) = \sqrt{\frac{1 - e^{-\xi}}{\xi}}. \quad (3.4)$$

Figure 3 shows the extracted value of $F(\xi)$ as a function of $\langle dN_{ch}/d\eta \rangle$ (N_{tracks}) from ALICE experiment for $\sqrt{s} = 5.02$ and 13 TeV using both estimator $SPD_{tracklets}$ and V0M. In case of $\sqrt{s} = 7$ TeV only V0M estimator results are shown. N_{tracks} is the charged particle multiplicity covering the pseudo-rapidity range $|\eta| < 0.8$ and $p_T = 0.15 - 20$ GeV/c [8]. It is observed that for fixed average charged particle multiplicity $F(\xi)$ has similar value for all three energies. Since $SPD_{tracklets}$ covers higher multiplicity further studies are shown only with this estimator. Figures 4 (a) and (b) show $F(\xi)$ and ξ as a function of $\langle dN_{ch}/d\eta \rangle$.

In case of $A-A$ collisions $\langle nS_1/S_n \rangle_{pp}^{mult}$ in Eqs. (3.2) and (3.3) is replaced by $\langle nS_1/S_n \rangle_{AA}$ and $F(\xi)_{AA}$ respectively. For Pb-Pb at $\sqrt{s_{NN}} = 2.76$ and 5.04 TeV and Xe-Xe at $\sqrt{s_{NN}} = 5.44$ TeV $F(\xi)$ has been extracted from the spectra at various centralities [10, 11]. Figures 5 (a) and (b) show $F(\xi)$ and ξ respectively for Xe-Xe and Pb-Pb collisions. To compare pp with the heavy ions results, we need to normalize N_{tracks} with the transverse area S_\perp in pp and $A-A$ collisions.

In pp collision $S_\perp = \pi R_{pp}^2$ has been computed in the IP-Glasma model, where R_{pp} is the interaction radius [41]. This is based on an impact parameter description of pp collisions, combined with an underlying description of particle production based on the theory of Color Glass Condensate [41]. The interaction radius R_{pp} is approximately a linear function of the charged particle multiplicity. In the IP-Glasma model R_{pp} is dependent on gluon multiplicity [41]

$$R_{pp} = f_{pp}(dN_g/dy)^{1/3}, \quad (3.5)$$

$$f_{pp} = \begin{cases} 0.387 + 0.0335x + 0.274x^2 - 0.0542x^3, & \text{if } x < 3.4, \\ 1.538 & \text{if } x \geq 3.4. \end{cases}$$

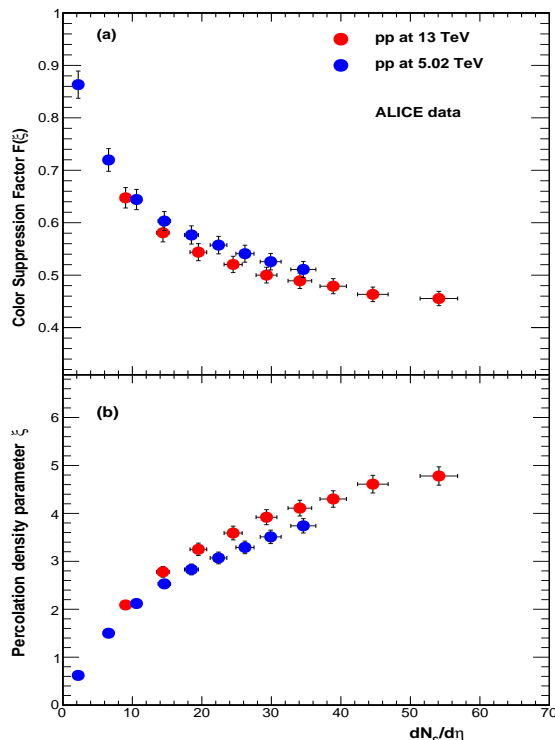


Figure 4. (a) Color suppression factor $F(\xi)$ and (b) String density ξ in pp collisions vs $dN_{ch}/d\eta$. $dN_{ch}/d\eta$ is the charged particle multiplicity covering the kinematic range $|\eta| < 0.8$ and $p_T = 0.15 - 20$ GeV/c [8].

where $x = (dN_g/dy)^{1/3}$. The gluon multiplicity dN_g/dy is related to the number of tracks seen in the CMS experiment by

$$dN_g/dy \approx (3/2) \frac{1}{\Delta\eta} N_{track} \quad (3.6)$$

where $\Delta\eta \sim 4.8$ units of pseudorapidity. The interaction cross section S_\perp for pp collisions at $\sqrt{s} = 5.02$ and 13 TeV from ALICE [8] is shown in Fig. 6. S_\perp increases with the multiplicity and for very high multiplicities it is approximately constant. In the case of A-A collisions the nuclear overlap area was obtained using the Glauber model. [42]. Figure 7(a) shows $F(\xi)$ as a function of $dN_{ch}/d\eta$ scaled by transverse area S_\perp for pp , Pb-Pb, and Xe-Xe collisions. Percolation density parameter ξ is shown in Fig. 7(b). Results are also shown for Au-Au collisions at $\sqrt{s}_{NN} = 200$ GeV [14]. A universal scaling behavior is observed in hadron-hadron and nucleus-nucleus collisions.

4 Connection between $F(\xi)$ and temperature

The connection between $F(\xi)$ and the temperature $T(\xi)$ involves the Schwinger mechanism (SM) for particle production. The Schwinger distribution for massless particles is expressed in terms of p_T^2 [33, 34]

$$dn/dp_T^2 \sim \exp(-\pi p_T^2/x^2) \quad (4.1)$$

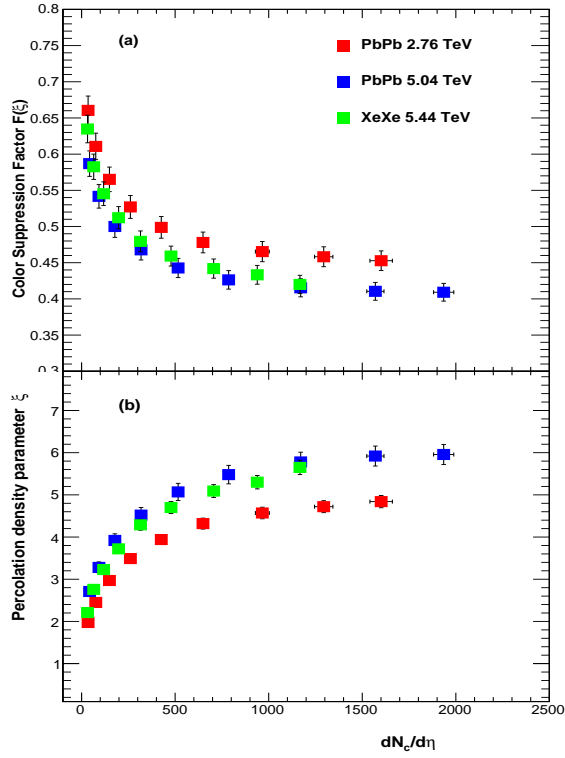


Figure 5. (a) Color suppression factor $F(\xi)$ and (b) String density ξ in Pb-Pb, and Xe-Xe collisions vs $dN_{ch}/d\eta$. $dN_{ch}/d\eta$ is the charged particle multiplicity covering the kinematic range $|\eta| < 0.8$ and $p_T = 0.15 - 20$ GeV/c [10, 11].

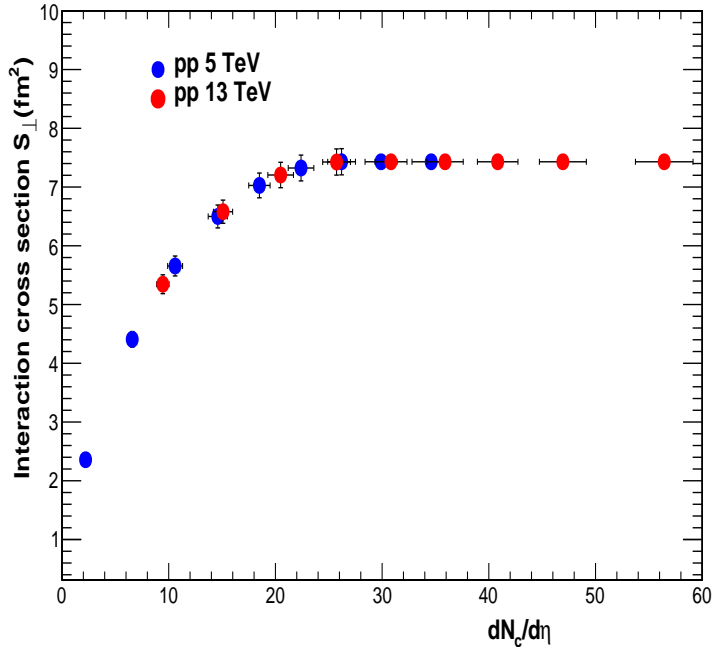


Figure 6. Interaction cross section S_{\perp} vs $dN_{ch}/d\eta$. S_{\perp} is obtained using IP-Glasma model [41].

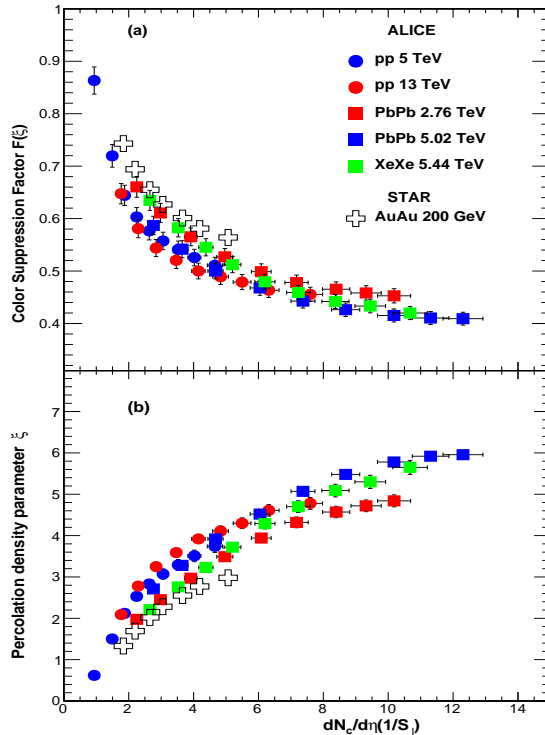


Figure 7. (a) Color Suppression Factor $F(\xi)$ in pp , Pb-Pb, and Xe-Xe collisions vs $dN_{ch}/d\eta$ scaled by the transverse area S_{\perp} . For pp collisions S_{\perp} is multiplicity dependent as obtained from IP-Glasma model [41]. In case of Pb-Pb and Xe-Xe collisions the nuclear overlap area was obtained using the Glauber model [42]. (b) String density parameter ξ . Results are also shown for Au-Au collisions at $\sqrt{s_{NN}} = 200$ GeV [14].

where the average value of the string tension is $\langle x^2 \rangle$. The tension of the macroscopic cluster fluctuates around its mean value because the chromo-electric field is not constant. The origin of the string fluctuation is related to the stochastic picture of the QCD vacuum. Since the average value of the color field strength must vanish, it cannot be constant but changes randomly from point to point [43, 44]. Such fluctuations lead to a Gaussian distribution of the string tension

$$\frac{dn}{dp_T^2} \sim \sqrt{\frac{2}{\langle x^2 \rangle}} \int_0^{\infty} dx \exp\left(-\frac{x^2}{2\langle x^2 \rangle}\right) \exp\left(-\pi \frac{p_T^2}{x^2}\right) \quad (4.2)$$

which gives rise to thermal distribution [43]

$$\frac{dn}{dp_T^2} \sim \exp\left(-p_T \sqrt{\frac{2\pi}{\langle x^2 \rangle}}\right), \quad (4.3)$$

with $\langle x^2 \rangle = \pi \langle p_T^2 \rangle_1 / F(\xi)$. The temperature is expressed as [14, 45]

$$T(\xi) = \sqrt{\frac{\langle p_T^2 \rangle_1}{2F(\xi)}}. \quad (4.4)$$

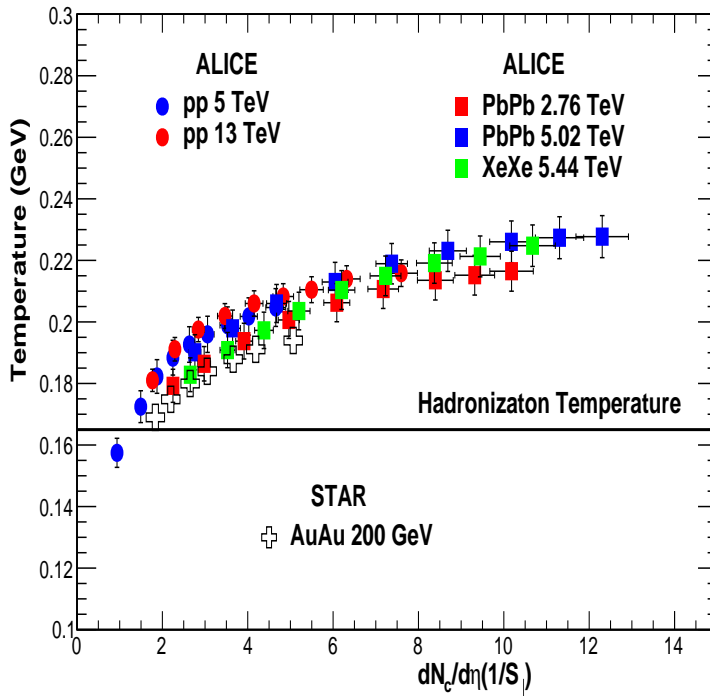


Figure 8. Temperature vs $dN_{ch}/d\eta$ scaled by S_{\perp} from pp , Pb-Pb, and Xe-Xe collisions. The horizontal line at ~ 165 MeV is the universal hadronization temperature [46].

The string percolation density parameter ξ which characterizes the percolation clusters measures the initial temperature of the system. Since this cluster covers most of the interaction area, the temperature becomes a global temperature determined by the string density. In this way at $\xi_c = 1.2$ the connectivity percolation transition at $T(\xi_c)$ models the thermal deconfinement transition.

Figure 8 shows the temperature as a function of $dN_c/d\eta$ scaled by the interaction area for pp , Xe-Xe, and Pb-Pb collisions at LHC energies. Temperature from both hadron-hadron and nucleus-nucleus collisions fall on a universal curve when multiplicity is scaled by the transverse interaction area. The horizontal line at ~ 167.7 MeV is the universal hadronization temperature obtained from the systematic comparison of the statistical thermal model parametrization of hadron abundances measured in high energy e^+e^- , pp , and $A-A$ collisions [46]. In Fig. 8 for pp collisions at $\sqrt{s} = 5.02$ and 13 TeV higher multiplicity cuts show temperatures above the hadronization temperature and similar to those observed in Au-Au collisions at $\sqrt{s_{NN}} = 200$ GeV [14].

It is observed that the temperature rises slowly at higher $dN_c/d\eta$ values. This behavior is related to the overlap area of strings, which is given by $(1 - e^{-\xi})$. Above $\xi \sim 4$ there is complete overlap and the temperature rises slowly as $\xi^{1/4}$. In Figs. 9(a) and (b) ξ and temperature are shown as a function of number of participants N_{part} . It is observed that

the string density ξ is collision energy dependent for the same number of participants.

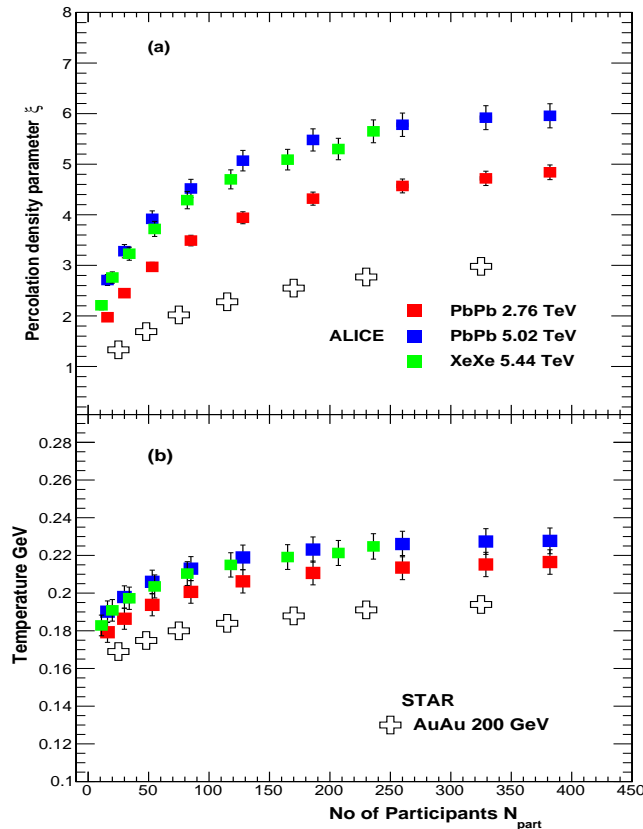


Figure 9. (a) Percolation density parameter ξ and (b) Temperature as a function of number of participants N_{part} in Pb-Pb and Xe-Xe collisions along with Au-Au at $\sqrt{s_{NN}} = 200$ GeV [14].

5 Thermalization

In case of $A - A$ collisions it was observed that average transverse momentum is twice the temperature $\langle p_T \rangle \sim 2T$ [12]. This shows that the charged particle transverse momentum spectrum is exponentially distributed, and the inverse slope parameter is the thermalized temperature [12]. Similar behavior is observed in pp collisions as shown in Fig. 10 along with Pb-Pb and Xe-Xe results.

The thermalization in pp and $A - A$ collisions can also occur through the existence of an event horizon caused by a rapid deceleration of the colliding nuclei [47, 48]. The thermalization is due to the Hawking-Unruh effect [47, 49, 50]. It is well known that the black holes evaporate by quantum pair production and behave as if they have an effective temperature of

$$T_H = \frac{1}{8\pi GM}, \quad (5.1)$$

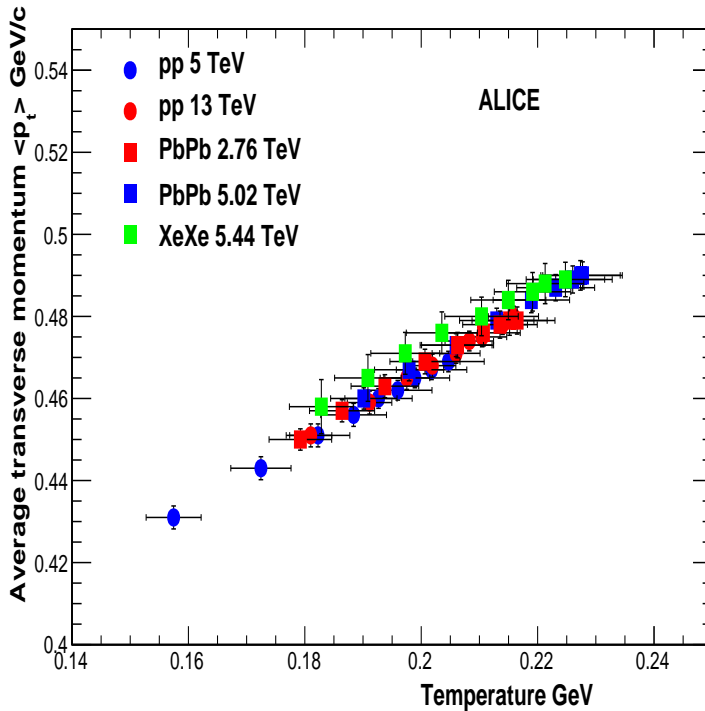


Figure 10. Average transverse momentum vs temperature.

where $1/4GM$ is the acceleration of gravity at the surface of a black hole of mass M . The rate of pair production in the gravitational background of the black hole can be evaluated by considering the tunneling through the event horizon. Unruh showed that a similar effect arises in a uniformly accelerated frame, where an observer detects the thermal radiation with the temperature $T = a/2\pi$, where a is the acceleration. Similarly, in hadronic interactions the probability to produce states of masses M due to the chromoelectric field E and color charge is given by the Schwinger mechanism [33]

$$W_M \sim \exp\left(\frac{-\pi M^2}{gE}\right) \sim \exp(-M/T), \quad (5.2)$$

which is similar to the Boltzmann weight in a heat bath with an effective temperature

$$T = \frac{a}{2\pi}, \quad a = \frac{2gE}{M}. \quad (5.3)$$

In CSPM the strong color field inside the large cluster produces deceleration of the primary $q\bar{q}$ pair which can be seen as a thermal temperature by means of the Hawking-Unruh effect. This implies that the radiation temperature is determined by the transverse extension of the color flux tube/cluster in terms of the string tension [47, 48, 51].

$$T = \sqrt{\frac{\sigma}{2\pi}} \quad (5.4)$$

The string percolation density parameter ξ which characterizes the percolation clusters measures the initial temperature via the color reduction factor $F(\xi)$. Since the cluster covers most of the interaction area, this temperature becomes a global temperature.

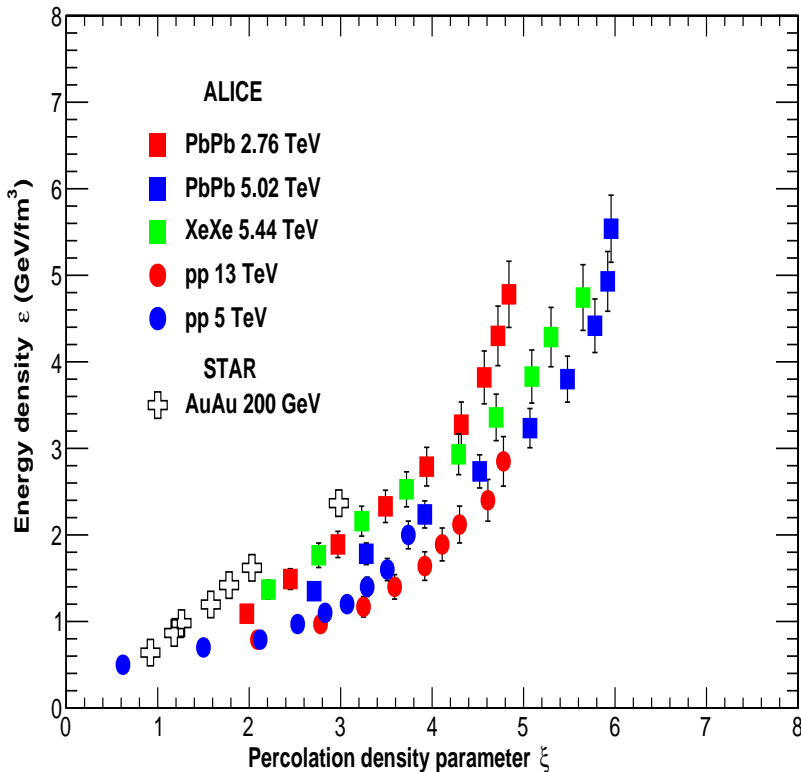


Figure 11. Energy density (ϵ) as a function of the percolation density parameter (ξ) for pp collisions at $\sqrt{s} = 5.02$ and 13 TeV, Pb-Pb collisions at $\sqrt{s_{NN}} = 2.76$ and 5.02 TeV, and Xe-Xe collisions at $\sqrt{s_{NN}} = 5.44$ TeV. Results from Au-Au collisions at $\sqrt{s_{NN}} = 200$ GeV are also shown [14].

6 Energy density

The QGP according to CSPM is born in local thermal equilibrium because the temperature is determined at the string level. After the initial temperature $T > T_c$ the CSPM perfect fluid may expand according to Bjorken boost invariant 1D hydrodynamics [52]

$$\epsilon = \frac{3}{2} \frac{dN_\epsilon}{dy} \langle m_T \rangle, \quad (6.1)$$

where ϵ is the energy density, S_n nuclear overlap area, m_T transverse mass and τ_{pro} the production time for a boson (gluon) [34]. τ_{pro} for a boson (gluon) is given by [33]

$$\tau_{pro} = \frac{2.405\hbar}{\langle m_T \rangle}. \quad (6.2)$$

Above the critical temperature only massless particles are present in CSPM. In Figure 11 energy density as a function of string density is shown for pp and $A - A$ collisions at LHC energies. Results for pp at $\sqrt{s} = 13$ TeV and Pb-Pb at $\sqrt{s_{NN}} = 2.76$ and 5.02 TeV are from our earlier publication [13]. Figure 11 also has results from Au-Au at $\sqrt{s_{NN}} = 200$ GeV [14]. We observe a slow rise of ϵ for low values of ξ followed by a faster rise later. It is found that ϵ is proportional to ξ in the range $1.2 < \xi < 5.0$. Above $\xi \sim 5$ the energy density ϵ rises faster compared to $\xi < 5$. A possible explanation for the sharp rise in the energy density could be that at such high degree of overlapping the gluons are seen naked without interaction and thus the coherence of the color fields of the overlapping strings is lost and thus recover the independence of the strings. This means that instead of a dependence on N_{part} it would be $N_{part}^{4/3}$.

It is worth mentioning that the CSPM is only used to encode the dependence on the centrality and energy of the temperature T given by the p_T spectrum. As far as this evaluation can be done directly from the p_T spectrum independently of the CSPM, our result can be seen independent of the model used.

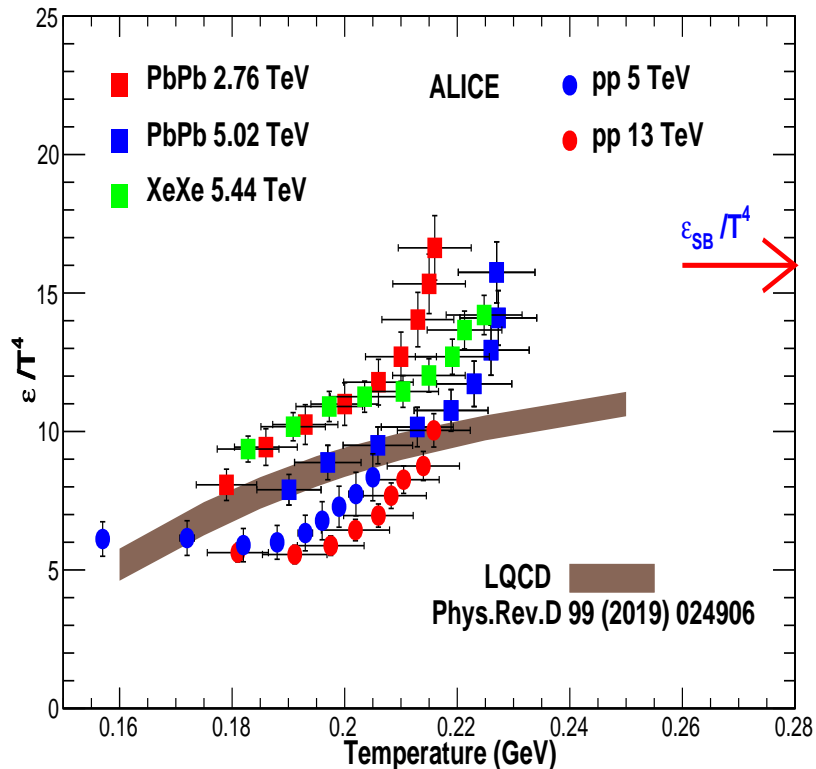


Figure 12. Dimensionless quantity ϵ/T^4 as a function of temperature from CSPM and LQCD calculation from HotQCD Collaboration [53]. The CSPM values at higher temperature $T > 200$ MeV are obtained extrapolating from lower temperature.

Energy density has been obtained in lattice set up of (2+1)-flavor QCD using the HISQ action and the tree-level improved gauge action [53, 54]. Figure 12 shows dimensionless quantity ε/T^4 as a function of temperature both from CSPM and LQCD. It is observed that CSPM results show similar trend with LQCD results up to the temperature of $T \sim 210$ MeV. Beyond this temperature the ε/T^4 in CSPM rises much faster and reaches the ideal gas value of $\varepsilon/T^4 \sim 16$ at $T \sim 230$ MeV. In this region, there is a strong screening due to the large degree of overlapping of the strings, producing a faster approach to the quark gluon gas limit.

To understand the behavior of ε/T^4 above ~ 210 MeV, one has to look at the energy density as a function of string density as shown in Fig. 13(a). The deviation from linearity start at $\xi \sim 5$. The CSPM values above $T \sim 210$ MeV have been obtained by extrapolating the linear fit to ε vs ξ up to $\xi \sim 5$ as shown in Fig. 13(a). Using the linear relation between ε and ξ one can obtain ε/T^4 as shown in Fig. 13(b). This extrapolation shows that the ε/T^4 trend seen in LQCD can be reproduced. It is worth noting that in CSPM the ideal gas limit is reached at lower temperature ~ 220 MeV while in LQCD ε/T^4 increases slowly towards the ideal gas limit.

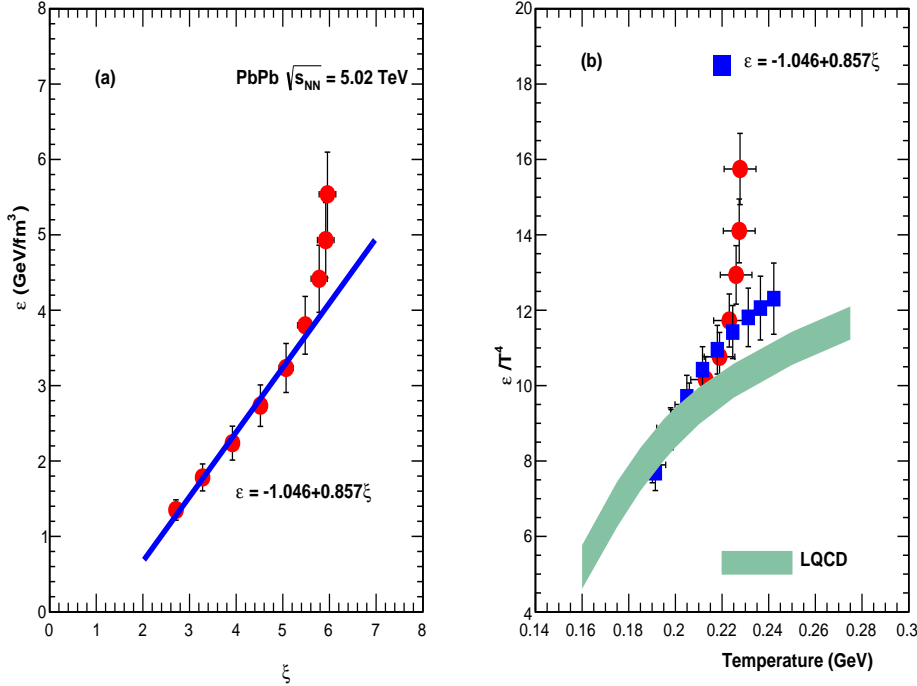


Figure 13. (a) Energy density ε vs percolation density parameter ξ . The line is a linear fit up to $\xi \sim 6$. (b) ε/T^4 vs temperature using linear fit from Fig. 13 (a). The LQCD results are from HotQCD Collaboration [53].

7 Two temperatures

In CSPM, we can associate two scales and the corresponding temperatures to the two different transitions. One is the string density required to have a large cluster of strings crossing the surface of the collision. This happens at the critical percolation density

$$\frac{N}{S_{\perp}} = \frac{\xi_c}{\pi r_0^2} \quad (7.1)$$

This corresponds to the hadronization temperature of the deconfinement. As the surface covered by strings is $(1 - \exp(-\xi))S_{\perp}$, the mean distance between strings d is

$$d = \left[\frac{N}{(1 - \exp(-\xi))S_{\perp}} \right]^{-1/2} = F(\xi)\sqrt{\pi}r_0. \quad (7.2)$$

For small ξ , $d > r_0$ for example at the critical percolation density $\xi_c = 1.2$, $d = 1.34r_0$. This means that overlapping between strings is very peripheral, covering only the edges (corona) of the strings. This corresponds to the hadronization temperature of ~ 166 MeV. In order to penetrate the core, the overlapping should be larger in such a way that $d < r_0$. In fact, for $d \sim 0.8 - 0.9r_0$, $F(\xi) \sim 0.45 - 0.51$ corresponding to the temperature of $\sim 208 - 220$ MeV. This is the temperature at which our result starts deviating from LQCD. These two temperatures can be seen, related to the confinement-deconfinement and possibly chiral symmetry restoration respectively.

8 Degrees of freedom DOF

In case of a quark-gluon system in thermal equilibrium at a high temperature the quarks and gluons are idealized to be non-interacting and massless and there is no net baryon number. The number of quarks and antiquarks are equal [34, 38]. The energy densities obtained in full QCD with different numbers of quark flavor are given by

$$\varepsilon/T^4 \simeq (37/30)\pi^2 \simeq 12, N_f = 2. \quad (8.1)$$

$$\varepsilon/T^4 \simeq (47.5/30)\pi^2 \simeq 16, N_f = 3. \quad (8.2)$$

At $T \sim 210$ MeV, $\varepsilon/T^4 \sim 11$ which corresponds to ~ 33 DOF while at $T \sim 230$ MeV there are ~ 47 DOF. In Fig. 12 Stefan-Boltzmann limit is also shown at ε_{SB}/T^4 , which corresponds to ~ 48 DOF. It is observed that Pb-Pb at $\sqrt{s_{NN}} = 2.76$ TeV has similar features as seen at 5.02 TeV. For Xe-Xe collisions at $\sqrt{s_{NN}} = 5.44$ TeV ~ 44 DOF is obtained. In pp collisions at $\sqrt{s} = 13$ TeV only ~ 33 DOF are reached. Our results agree with the conclusions obtained studying the trace anomaly in a quasi particle gluonic model [55, 56]. In this model the DOF of the free gluons are also obtained for $T \simeq 1.3T_c$ ($T_c \approx 165$ MeV).

9 Discussion

The most pressing question to be addressed is the appearance of a transition in CSPM at $T \sim 210$ MeV above the deconfinement transition. It is quite possible that temperature ~ 210 MeV is the chiral symmetry restoration temperature. In that case the deconfinement temperature occurs at lower temperature than the chiral symmetry restoration temperature. However, the LQCD calculation of equation of state in 2+1 flavor QCD at finite temperature finds that deconfinement and chiral symmetry restoration occur in the same temperature range i.e., in a region of the QCD phase transition where the transition is not a true phase transition rather a rapid crossover [57].

It has been suggested chiral symmetry restoration occurs either together with or after color deconfinement [38]. Deconfinement is the transition from a state of color-neutral hadrons to one of the colored quarks. Chiral symmetry restoration is the transition from a state of massive “dressed” constituent quarks to one of massless current quarks. These two phenomena need not coincide [38, 58].

A new phase in QCD also has been proposed studying the Dirac operator [59]. While confining chromo-electric interaction is distributed among all modes of Dirac operator, the chromo-magnetic interaction is located predominantly in the near zero modes. Above $T \sim 155$ MeV the near zero modes are suppressed but not the rest of the modes, surviving the chromo-electric interaction which is suppressed at higher temperature [59]. Following this, it has been conjectured that the intermediate temperature regime is “stringy fluid” where chiral symmetry is stored [60].

Recently, it has been pointed out using lattice simulations that in addition of the standard crossover phase transition at $T \sim 155$ MeV, the existence of a new infrared phase transition at temperature T , $200 < T_{IR} < 250$ MeV. In this phase, asymptotic freedom works and therefore there is no interaction. In between these two temperatures there is possible coexistence of the short and long-distance scales [61, 62], which supports the present observation in our work.

Chiral symmetry restoration also has been studied by an accelerating observer considering the Unruh effect. As a result, it is shown that chiral symmetry is restored for uniformly accelerated observers with acceleration \mathbf{a} larger than the critical value $a_c = 4\pi f_\pi$, with f_π being pion decay constant [63].

10 Conclusions

We have used the Color String Percolation Model (CSPM) to explore the initial stage in pp , Xe-Xe, and Pb-Pb collisions at LHC energies and determined the thermalized initial temperature of the hot nuclear matter at an initial time ~ 1 fm/c. For the first time both the temperature and the energy density of the hot nuclear matter have been obtained from the measured charged particle spectra using ALICE data for pp collisions at $\sqrt{s} = 5.02$ and 13 TeV. In $A - A$ collisions Pb-Pb at $\sqrt{s_{NN}} = 5.02$ and 5.44 TeV along with at Xe-Xe $\sqrt{s_{NN}} = 5.44$ TeV have been used. A universal scaling in the temperature is obtained for both pp and $A - A$ (Fig. 8) and are well above the universal hadronization temperature

indicating that the matter created is in the deconfined phase. The thermalization in both pp and $A - A$ is reached through the stochastic process (Hawking-Unruh) rather than the kinetic approach.

The dimensionless quantity ε/T^4 is evaluated to obtain the number of degrees of freedom (DOF) of the deconfined phase. We observe two features hitherto not reported: the existence of two temperature ranges in the behavior of the $A - A$ system DOF, and a clear departure from the LQCD results regarding the maximum number of DOF, which reaches values in agreement with the Stephan Boltzmann limit for an ideal gas of quarks and gluons. In case of pp collisions at $\sqrt{s} = 5.02$ we reach only $\varepsilon/T^4 \sim 8$ corresponding to ~ 24 DOF, while at $\sqrt{s} = 13$ TeV ~ 30 DOF is obtained. There are several reasons that can explain the disagreement between CSPM and lattice QCD for $T > 1.3T_c$. First, in $A - A$ and pp collisions a strong magnetic field B is produced, which is larger for $A - A$ than for pp and increases with energy. The lattice studies of the chiral phase structure of three flavor QCD in a background magnetic field show that chiral condensate and the phase transition temperature always increases with B . The transition becomes stronger and turns into a first order instead of crossover [64]. As B is higher in Pb-Pb than in pp , we expect a higher phase transition temperature in these cases.

It has been argued that QCD could lead to a three-phase structure as a function of the temperature. In such a scenario, color deconfinement would result in a plasma of massive “dressed” quarks; the only role of gluons in this state would be to dynamically generate the effective quark mass. The effective DOF in the resulting quark plasma thus are just those of massive quarks. At still higher temperature, this gluonic dressing of quarks would then evaporate, leading to QGP, with restored chiral symmetry [1, 38]. Our results show that the chiral symmetry restoration occurs ~ 210 MeV. Beyond this temperature ε/T^4 rises much faster and reaches the Stefan-Boltzmann limit $\varepsilon/T^4 \sim 16$ at $T \sim 230$ MeV.

11 Acknowledgments

A. M. thanks the Hungarian National Research, Development and Innovation Office (NK-FIH) under the contract numbers OTKA K135515, K123815, 2019-2.1.11-T ET-2019-00078, 2019-2.1.11-TET-2019-00050, and Wigner Scientific Computing Laboratory (WSCLAB, the former Wigner GPU Laboratory). G.P. work is supported by the grant from CONACYT under the grant A1-S-22917 and CF-2042. C.P. thanks the grant Maria de Maeztu Unit of excellence MDM-2016-0682 of Spain, the support of Xunta de Galicia under the project ED431C 2017 and project PID 2020-119632GB-IOO of Ministerio de Ciencia e Innovacion of Spain and FEDER.

References

- [1] P. Castorina, R. V. Gavai, and H. Satz, The QCD phase structure at high baryon density, *Eur. Phys. J.* **C 69** (2010) 169.
- [2] W. Busza, K. Rajagopal, and W. van der Schee, Heavy ion collisions: The Big Picture, and the Big Questions, *Ann. Rev. Nucl. Part. Sci.* **68** (2018) 339.

- [3] V. Khachatryan et al. (CMS Collaboration), Observation of long range near-side angular correlations in pp collisions at LHC, *JHEP* **09** (2010) 091.
- [4] V. Khachatryan et al. (CMS Collaboration), Measurement of long range near side two particle angular correlations in pp collisions at $\sqrt{s} = 13$ TeV , *Phys. Rev. Lett.* **116** (2016) 172302.
- [5] V. Khachatryan *et al.* (CMS Collaboration), Evidence of collectivity in pp collisions at the LHC, *Phys. Lett.* **B 765** (2017) 193.
- [6] G. Aad et al. (ATLAS Collaboration), Observation of long range elliptic azimuthal anisotropies in $\sqrt{s} = 13$ and 2.76 TeV pp collisions with the ATLAS detector, *Phys. Rev. Lett.* **116** (2016) 172301.
- [7] J. Adam *et al.* (ALICE Collaboration), Enhanced production of multi-strange hadrons in high-multiplicity proton-proton collisions, *Nature Physics* **13** (2017) 535.
- [8] S. Acharya *et al.* (ALICE Collaboration), Charged particle production as a function of multiplicity and transverse sphericity in pp collisions at $\sqrt{s} = 5.02$ and 13 TeV, *Eur. Phys. J. C* **79** (2019) 857.
- [9] S. Acharya *et al.* (ALICE Collaboration), Multiplicity dependence of light-flavor hadron production in *pp* collisions at $\sqrt{s} = 7$ TeV, *Phys. Rev. C* **99** (2019) 024906.
- [10] J. Acharya *et al.* (ALICE Collaboration), Transverse momentum spectra and nuclear modification factors of charged particles in pp, p-Pb and Pb-Pb collisions at the LHC, *JHEP* **11** (2018) 013.
- [11] J. Adam *et al.* (ALICE Collaboration), Transverse momentum spectra and nuclear modification factors of charged particles in Xe-Xe collisions at $\sqrt{s_{NN}} = 5.44$ TeV, *Phys. Lett.* **B 788** (2019) 166.
- [12] M. A. Braun, J. D. de Deus, A. S. Hirsch, C. Pajares, R. P. Scharenberg, and B. K. Srivastava, Deconfinement and clustering of color sources in nuclear collisions, *Phys. Rep.* **599** (2015) 1.
- [13] A. N. Mishra, G. Paic, C. Pajares, R. P. Scharenberg, and B. K. Srivastava, Deconfinement and degrees of freedom in *pp* and A-A collisions at LHC energies, *Eur. Phys. J. A* **57** (2021) 245.
- [14] R. P. Scharenberg, B. K. Srivastava and A. S. Hirsch, Percolation of color sources and the equation of state of QGP in central Au-Au collisions at $\sqrt{s_{NN}} = 200$ GeV, *Eur. Phys. J. C* **71** (2011) 1510.
- [15] J. Dias de Deus, A. S. Hirsch, C. Pajares, R. P. Scharenberg and B. K. Srivastava, Clustering of color sources and the shear viscosity of the QGP in heavy ion collisions at RHIC and LHC energies, *Eur. Phys. J. C* **72** (2012) 2123.
- [16] B. K. Srivastava, Percolation approach to initial stage effects in high energy collisions, *Nucl. Phys. A* **926** (2014) 142.
- [17] J. Dias de Deus, A. S. Hirsch, C. Pajares, R. P. Scharenberg and B. K. Srivastava, Transport coefficient to trace anomaly in the clustering of color sources approach, *Phys. Rev. C* **93** (2016) 024915.
- [18] R. P. Scharenberg, The QGP equation of state by measuring the color suppression factor at RHIC and LHC energies, *PoS (CPOD 2013)* **017** (2013).

- [19] R. P. Scharenberg, B. K. Srivastava, and C. Pajares, Exploring the initial stage of high multiplicity proton-proton collisions by determining the initial temperature of quark-gluon plasma, *Phys. Rev. D* **100** (2019) 114040.
- [20] L. Cunqueiro, J. Dias de Deus, and C. Pajares, Nuclear-like effects in proton-proton collisions at high energy, *Eur. Phys. J. C* **65** (2010) 423.
- [21] C. Andres, A. Moscoso and C. Pajares, On the onset of ridge structure in AA, pA and pp collisions , *Phys. Rev. C* **90** (2014) 054902 .
- [22] P. Sahoo et al., Energy and centrality dependent study of deconfinement phase transition in a color string percolation approach at RHIC energies, *Eur. Phys. J. A* **54** (2018) 136.
- [23] P. Sahoo et al., Electrical conductivity of hot and dense QCD matter created in heavy-ion collisions: A color string percolation approach , *Phys. Rev. D* **98** (2018) 054005.
- [24] P. Sahoo et al., Thermodynamic and transport properties in Au+Au collisions at RHIC energies from the clustering of color strings, *Mod. Phys. Lett. A* **34** (2019) 1950034.
- [25] C. Bierlich, G. Gustafson, L. Lonnald, and A. Tarasov, Effects of overlapping strings in *pp* collisions, *JHEP* **03** (2015) 58.
- [26] C. Bierlich, G. Gustafson, and L. Lonnald, Collectivity without plasma in hadronic collisions, *Phys. Lett. B* **779** (2018) 58.
- [27] A. Ortiz Velasquez, P. Christiansen, E. Cuautle Flores, I. A. Maldonado, and G. Paic, Color reconnection and flowlike patterns in *pp* collisions, *Phys. Rev. Lett.* **111** (2013) 042001.
- [28] M. Asakawa, S. A. Bass, and B. Muller, Center domains and their phenomenological consequences, *Phys. Rev. Lett.* **110** (2013) 202301 .
- [29] A. Dumitru, T. Lappi, and Y. Nara, Structure of longitudinal chromomagnetic fields in high energy collisions, *Phys. Lett. B* **734** (2014) 7.
- [30] A. Bazavov, P. Petreczky, and J. H. Weber, Equation of state in 2+1 flavor QCD at high temperatures, *Phys. Rev. Lett.* **97** (2018) 014510.
- [31] M. A. Braun and C. Pajares, Implications of color-string percolation on multiplicities, correlations, and the transverse momentum, *Eur. Phys. J. C* **16** (2000) 349.
- [32] M. A. Braun, F. del Moral and C. Pajares, Percolation of strings and the relativistic energy data on multiplicity and transverse momentum distributions, *Phys. Rev. C* **65** (2002) 024907.
- [33] J. Schwinger, Gauge variance and mass II, *Phys. Rev.* **128** (1962) 2425.
- [34] C Y. Wong, *Introduction to high energy heavy ion collisions* (1994) 289.
- [35] R. Ryblewski and W. Florkowski, Equilibration of anisotropic quark-gluon plasma produced by decay of color flux tubes, *Phys. Rev. D* **88** (2013) 034028.
- [36] M. Ruggieri et al., Modeling early stages of relativistic heavy ion collisions: Coupling relativistic transport theory to decaying color-electric flux tubes, *Phys. Rev. C* **92** (2015) 064904.
- [37] M. B. Isichenko, Percolation, statistical topography, and transport in random media, *Rev. Mod. Phys.* **64** (1992) 961.
- [38] H. Satz, *Extreme states of matter in strong interaction physics, Lecture notes in physics 945* (Springer International Publishing AG, Berlin,2018)

- [39] L. McLerran, and R. Venugopalan, Computing quark and gluon distribution functions for very large nuclei, *Phys. Rev. D* **49** (1994) 2233.
- [40] J. D. Dias de Deus, C. Pajares, String percolation and the Glasma, *Phys. Lett. B* **695** (2011) 211.
- [41] L. McLerran, M. Praszalowicz, and B. Schenke, Transverse momentum of protons, pions and kaons in high multiplicity pp and pA collisions; evidence of the Color Glass Condensate ?, *Nucl. Phys. A* **916** (2013) 210.
- [42] C. Loizides, Glauber modeling of high-energy nuclear collisions at the subnucleon level, *Phys. Rev. C* **94** (2016) 024914.
- [43] A. Bialas, Fluctuations of the string tension and transverse mass distribution, *Phys. Lett. B* **466** (1999) 301.
- [44] H. G. Dosch, Gluon condensate and effective linear potential, *Phys. Lett. B* **190** (1987) 177.
- [45] J. Dias de Deus and C. Pajares, Percolation of color sources and critical temperature, *Phys. Lett. B* **642** (2006) 455.
- [46] F. Becattini, P. Castorina, A. Milov, and H. Satz, A comparative analysis of statistical hadron production, *Eur. Phys. J. C* **66** (2010) 377.
- [47] P. Castorina, D. Kharzeev, and H. Satz, Thermal hadronization and Hawking-Unruh radiation in QCD, *Eur. Phys. J. C* **52** (2007) 187.
- [48] A. A. Bylinkin, D. E. Kharzeev, and A. A. Rostovtsev, The origin of thermal component in the transverse momentum spectra in high energy hadronic processes, *Int. J. Mod. Phys. E* **23** (2014) 1450083.
- [49] S. W. Hawking, Particle creation by black hole, *Commun. Math. Phys* **43** (1975) 199.
- [50] W. G. Unruh, Notes on black-hole evaporation, *Phys. Rev. D* **14** (1976) 870.
- [51] P. Castorina and H. Satz, Hawking-Unruh hadronization and strangeness production in high energy collisions, *Adv. High. Ener. Phys. C* **52** (2014) 376982.
- [52] J. D. Bjorken, Highly relativistic nucleus-nucleus collisions: The central rapidity region, *Phys. Rev. D* **27** (1983) 140.
- [53] A. Bazavov et al., Equation of state in (2+1)-flavor QCD, *Phys. Rev. D* **90** (2014) 094503 .
- [54] B. Borsanyi *et al.* (Wuppertal Collaboration), Full result for the QCD equation of state with 2+1 flavors, *Phys. Lett. B* **730** (2014) 99.
- [55] P. Castorina and M. Mannarelli, Effective degrees of freedom of the quark-gluon plasma, *Phys. Lett. B* **644** (2007) 336.
- [56] P. Castorina and M. Mannarelli, Effective degrees of freedom and gluon condensation in the high temperature deconfined phase, *Phys. Rev. C* **75** (2007) 054901.
- [57] A. Bazavov et al., Equation of state and QCD transition at finite temperature, *Phys. Rev. D* **80** (2009) 014504.
- [58] J. Kogut et al., Scales of chiral symmetry breaking in quantum chromodynamics, *Phys. Rev. Lett.* **48** (1982) 1140.
- [59] Three regimes of QCD, L. Ya. Glozman, Three regimes of QCD, arXiv:1907.018201.

- [60] Jon-Ivar Skullerud, QCD at high temperature and density :selected highlights, arXiv:2112.07595.
- [61] A. Alexandru and I. Horváth, Possible new phase of thermal QCD, Phys. Rev. D **100** (2019) 094507.
- [62] A. Alexandru and I. Horváth, Unusual features of QCD low-energy modes in IR phase, Phys. Rev. Lett. **127** (2021) 052303.
- [63] Adrián Casado-Turrión and Antonio Dobado, Triggering the QCD phase transition through the Unruh effect: chiral symmetry restoration for uniformly accelerated observers, Phys. Rev. D **99** (2019) 125018.
- [64] H. T. Ding et al., Chiral phase structure of three flavor QCD in a background magnetic field, Phys. Rev. D **102** (2020) 054505.